COMPRESSION OF EIGENVALUE RANGE BY USING A SURPLUS OF ADAPTIVE ANTENNA ELEMENTS

Hakim Mesiwala and Bernard Widrow
Department of Electrical Engineering, Stanford University
Stanford, CA 94305

SUMMARY

This paper demonstrates that the addition and judicious placement of a few extra antenna elements speeds up convergence of the nulling process for an adaptive antenna array that is subjected to closely spaced jammers of disparate power levels.

An added benefit resulting from this reconfiguration is increased sharpness of the notches in the receiving directivity pattern at the jammer positions and omnidirectionality of the pattern elsewhere.

I. INTRODUCTION

Adaptive antenna array systems have been used to steer nulls in the direction of arrival of interfering signals called jammers.[1] Previous analyses and simulations relating to these adaptive null steerers have focused attention on nulling of a single jammer or of multiple jammers with equal power and with wide angular separation.[2,3,4]

When two or more jammers with widely differing power levels are involved, the time required to null† all jammers becomes very long in comparison with the time required to null a single jammer. This problem has been pointed out by White[5] and Reed *et al.*[6]

The purpose of the research reported in this paper is to demonstrate the effectiveness of adding extra antenna elements to the adaptive null steerer (ANS) in order to speed up the adaptive nulling process for two closely spaced jammers with disparate power levels.

II. DEMONSTRATION OF THE PROBLEM

To demonstrate the slowness in the nulling process, a minimal structure (Fig. 1) with one primary element and two auxiliary elements is employed to null two jammers designated as follows:

J_1 = Jammer 1 with power 100, incident at 40^o as shown in the figure.

J_2 = Jammer 2 with power 1, incident at 55^o.

The angular position of J_1 is chosen rather arbitrarily, while that of J_2 is chosen reasonably close to J_1.

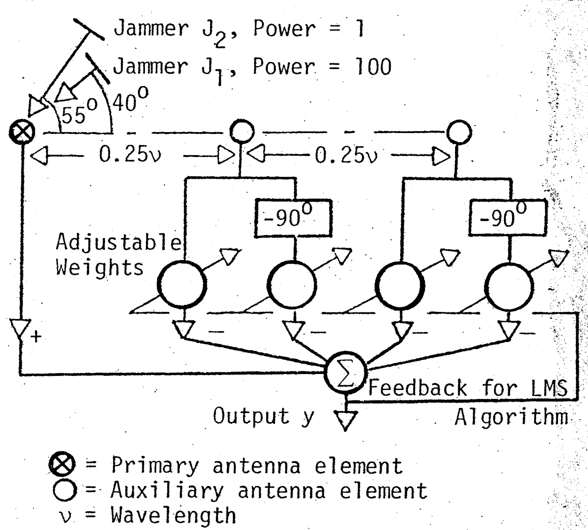

Fig. 1. A minimal Adaptive Null Steerer (ANS) to null 2 jammers.

To focus attention on the essence of the problem, it is assumed that the jammers are narrowband signals which may be approximated by sinusoids. Thus 90^o phase shifters (instead of tapped delay lines) are used on each auxiliary antenna element. The LMS adaptive algorithm[7] is used in a simulation involving the configuration of Fig. 1. After a few adaptations the weights are frozen and the resulting antenna beam pattern‡ is plotted. Then the adaptive process is resumed and the pattern plotting procedure is repeated at frequent intervals. It may be noted that no noise is added to the signals in order to concentrate exclusively on the convergence problems due to the jamming signals only.

This work was supported by Naval Air Systems Command Code Air 310B under Contract No. N00019-78-C-0276.

†To attenuate severely.

‡The beam pattern is the array response to a unit power test signal which is swept over 360^o while keeping the adjustable weights frozen.

Figures 2a through 2d show a time sequence of beam patterns achieved by the above simulation as adaptation proceeds. The arrows in the figure indicate the positions of the jammers.

From Fig. 2a it is clear that the high-power jammer is nulled quickly, but the low-power jammer is essentially unaffected. In Fig. 2b the pattern has changed substantially; but it shows little nulling effect in the area of the low-power jammer. After about 40,000 adapts the low-power signal begins to be nulled as shown in Fig. 2c. Well formed nulls begin to occur after about 70,000 adapts. Good nulls are achieved by about 120,000 adapts. For the purpose of this paper convergence may be defined as the minimum number of adapts needed to reduce the output power to below 1×10^{-6}. For the configuration in Fig. 1 this occurs around 141,000 iterations. The converged† pattern is shown in Fig. 2d.

In passing it may be mentioned that the beam patterns are symmetrical about 0^o because a line array of antenna elements is unable to distinguish positive from negative angular positions.

The sluggishness of the adaptive array in nulling the low-power jammer may be explained with the aid of the analysis presented in the following section.

III. ANALYSIS RELATING TO CONVERGENCE RATE OF ADAPTIVE ARRAYS

A generalized version of the adaptive antenna array of Fig. 1 is shown in Fig. 3. The k^{th} auxiliary element is located at a distance ℓ_k (given in units of wavelengths) from the primary element at an angle α_k with an arbitrary reference axis. Two jammers (J_1 and J_2) with powers ρ_1 and ρ_2 (at each antenna element) arrive at angles ψ_1 and ψ_2 as shown in the figure.

Central to the analysis of the adaptive linear combiner of the type used in Fig. 3 is the correlation matrix R (Widrow et al)[7] defined by

$$R \triangleq [E(x_{i1}x_{i2})] \tag{1}$$

where $E(x_{i1}x_{i2})$ is the statistical correlation

† The converged pattern is defined as the beam pattern obtained after the convergence of the algorithm.

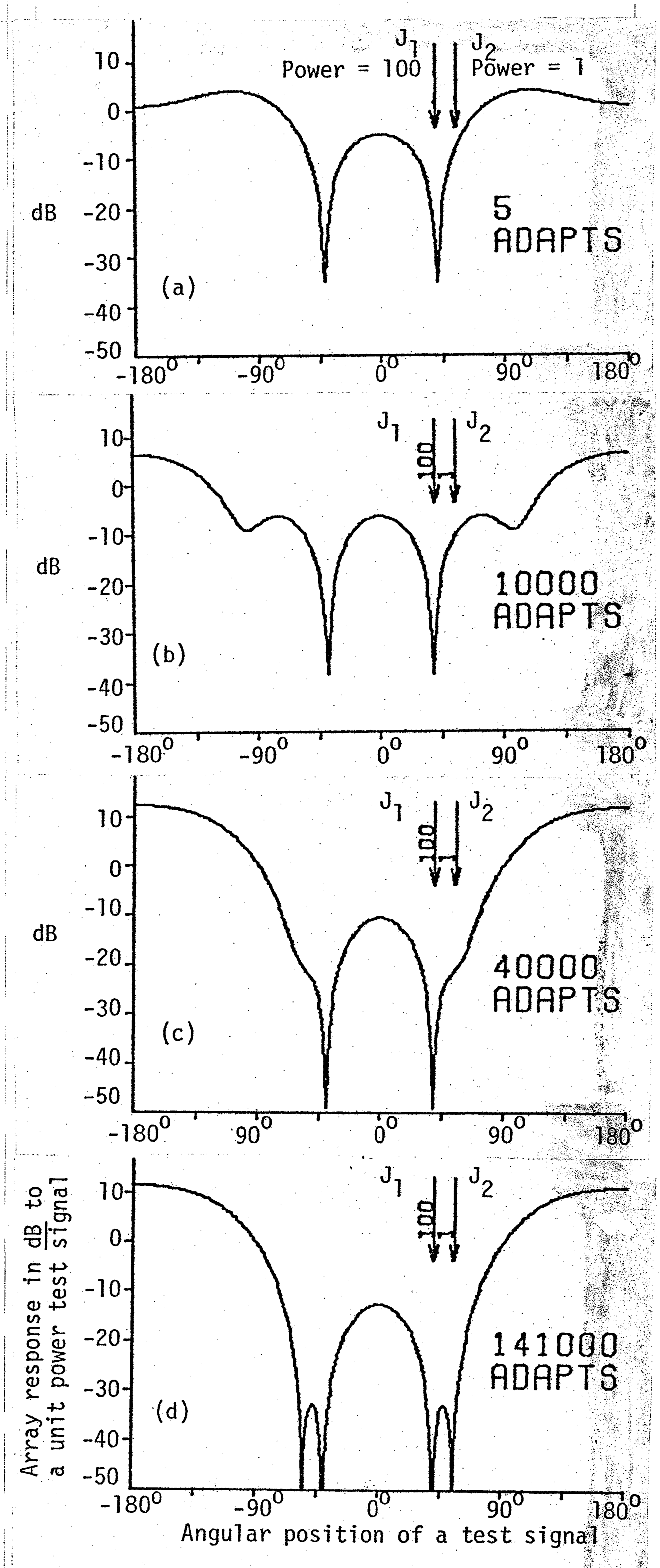

Fig. 2. A time sequence of beam patterns for the ANS of Fig. 1.

between the signals x_{i1} and x_{i2} where i1, i2 = 1, 2, ..., 2n. The speed of convergence is intimately related to the eigenvalues of R, as can be seen from the following.

For stability of the LMS adaptive algorithm [see (24) of Widrow[7]] the adaptation constant μ must satisfy

$$1/\lambda_{max} > \mu > 0 \tag{2}$$

where $\lambda_{max} \stackrel{\Delta}{=}$ maximum eigenvalue of the R matrix.

The dynamics of an adaptive system depend only on the nonzero eigenvalues of R. For every nonzero eigenvalue λ, the time constant τ of the corresponding mode is given by [see (27) of Widrow[7]]

$$\tau = 1/2\mu\lambda \quad . \tag{3}$$

(τ is dimensionless. It is expressed in number of adapts.)

The time for convergence is thus determined by the minimum nonzero eigenvalue λ_{min}. From (3):

$$\tau_{max} = 1/2\mu\lambda_{min} \quad . \tag{4}$$

Using the inequality (2):

$$\tau_{max} > \lambda_{max}/2\lambda_{min} \quad . \tag{5}$$

In practice the μ is required to be very small compared with $1/\lambda_{max}$ to keep the misadjustment† within an acceptable limit. Therefore τ_{max} is much greater than that indicated by the lower bound, which is the right hand side (RHS) of (5). Nevertheless, the ratio $\lambda_{max}/\lambda_{min}$ in the RHS of (5) gives a good measure for comparison of speed of convergence, as will be seen from the examples discussed in sections IV and V.

From a detailed analysis given in the appendix it is shown that the eigenvalues (for the general case in Fig. 3) are

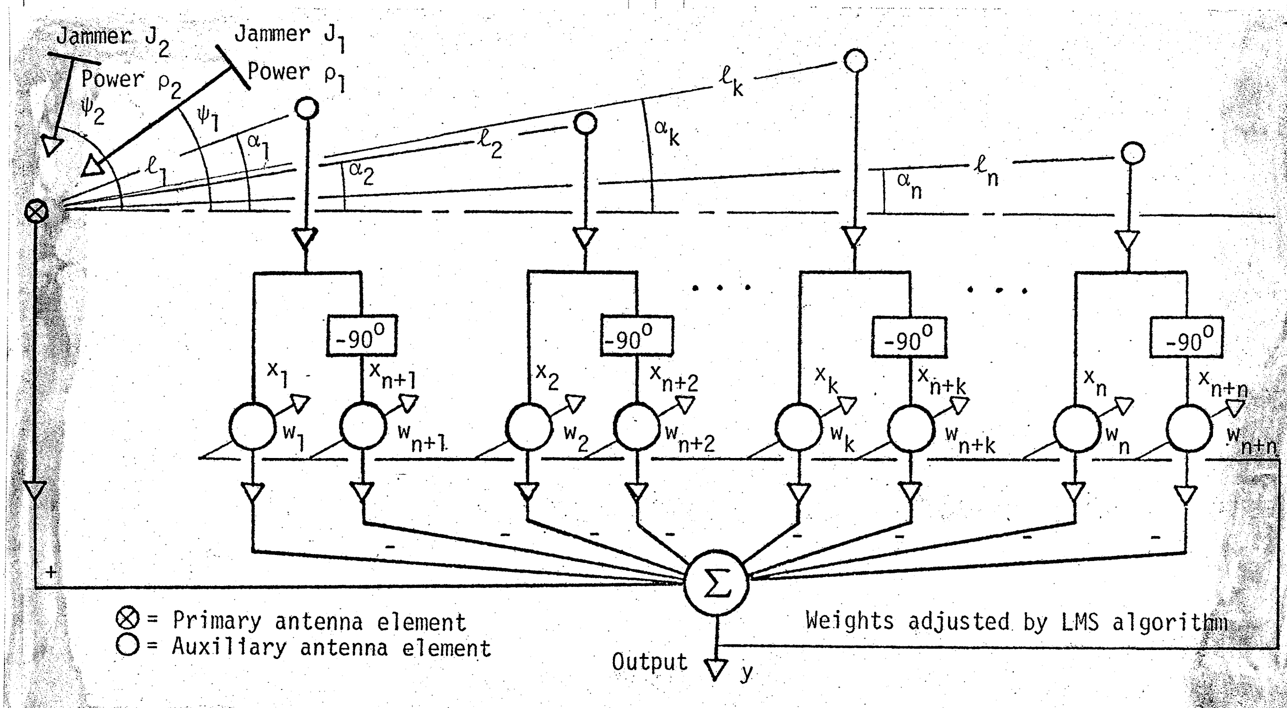

Fig. 3. An Adaptive Null Steerer with one primary and n auxiliary antenna elements.

---

†Misadjustment[7] $\quad M \stackrel{\Delta}{=} \dfrac{\text{Average excess mean squared error (mse)}}{\text{mse obtained with optimum weight setting}}$

$$
\left.\begin{aligned}
\lambda_1 &= \frac{n}{2}(\rho_1+\rho_2) + \left[\frac{n^2}{4}(\rho_1-\rho_2)^2+\rho_2\rho_1|U_1^*U_2|^2\right]^{\frac{1}{2}} \\
\lambda_2 &= \frac{n}{2}(\rho_1+\rho_2) - \left[\frac{n^2}{4}(\rho_1-\rho_2)^2+\rho_2\rho_1|U_1^*U_2|^2\right]^{\frac{1}{2}} \\
\lambda_{n+1} &= \lambda_1; \quad \lambda_{n+2} = \lambda_2 \\
\lambda_m &= 0 \quad \text{for} \quad m \notin \{1,2,n+1,n+2\} \\
&\text{where} \\
U_j &\triangleq \left[e^{-i\phi_{1j}}, e^{-i\phi_{2j}}, \ldots, e^{-i\phi_{nj}}\right]^T \\
&j = 1,2 \text{ (jammer index)} \\
U_1^* &\triangleq \text{Complex conjugate transpose of } U_1 \\
\phi_{kj} &\triangleq 2\pi\ell_k \cos(\psi_j-\alpha_k) \\
&k = 1,\ldots,n \text{ (auxiliary element index)} \\
\ell_k &\triangleq \text{distance of } k^{th} \text{ antenna element from the primary antenna element } (\ell_k \text{ given in units of wave length), and} \\
\alpha_k &= \text{Angle of } k^{th} \text{ element with respect to the reference axis (see Fig. 3).}
\end{aligned}\right\} \quad (6)
$$

The ratio of maximum eigenvalue to minimum nonzero eigenvalue is thus given by

$$
\frac{\lambda_{max}}{\lambda_{min}} = \frac{\lambda_1}{\lambda_2} = \frac{\dfrac{(\rho_1+\rho_2)}{2} + \left[\dfrac{(\rho_1-\rho_2)^2}{4} + \rho_1\rho_2 \dfrac{|U_1^*U_2|^2}{n^2}\right]^{\frac{1}{2}}}{\dfrac{(\rho_1+\rho_2)}{2} - \left[\dfrac{(\rho_1-\rho_2)^2}{4} + \rho_1\rho_2 \dfrac{|U_1^*U_2|^2}{n^2}\right]^{\frac{1}{2}}} \quad . \quad (7)
$$

From the definition of U_j in (6) it is seen that $|U_1^*U_2|$ varies between 0 and n. Thus for given ρ_1 and ρ_2 ($\rho_1 \geq \rho_2$), the ratio $\lambda_{max}/\lambda_{min}$ varies between ρ_1/ρ_2 and ∞. $\lambda_{max}/\lambda_{min}$ must be kept small in order to keep τ_{max} small [see (5)]. Therefore the number of elements and their geometrical arrangement in the array are to be chosen such that the ratio $\lambda_{max}/\lambda_{min}$ is kept near ρ_1/ρ_2 for most ψ_1 and ψ_2 of practical interest. (Note that $\psi_1 \to \psi_2 \Rightarrow \phi_{k1} \to \phi_{k2} \Rightarrow U_1 \to U_2 \Rightarrow |U_1^*U_2| \to n$ which implies from (7) that $\lambda_{max}/\lambda_{min} \to \infty$.)

To obtain a better understanding of the implications of (6) and (7), compare two special classes, namely:

(i) $\rho = \rho_1 = \rho_2$.

Substituting in (6) and (7) yields

$$
\left.\begin{aligned}
\lambda_1 &= \lambda_{n+1} = \rho(n + |U_1^*U_2|) \\
\lambda_2 &= \lambda_{n+2} = \rho(n - |U_1^*U_2|) \\
\lambda_m &= 0 \quad \text{otherwise} \quad .
\end{aligned}\right\} \quad (8)
$$

$$
\frac{\lambda_{max}}{\lambda_{min}} = \frac{1 + |U_1^*U_2|/n}{1 - |U_1^*U_2|/n} \quad . \quad (9)
$$

(ii) $\rho_1 >> \rho_2$.

Making first-order approximations in (6) and (7) it can be seen that

$$
\left.\begin{aligned}
\lambda_1 &= \lambda_{n+1} \simeq n\rho_1 \\
\lambda_2 &= \lambda_{n+2} \simeq n\rho_2\left[1 - \frac{|U_1^*U_2|^2}{n^2}\right] \\
\lambda_m &= 0 \quad \text{otherwise} \quad .
\end{aligned}\right\} \quad (10)
$$

$$
\frac{\lambda_{max}}{\lambda_{min}} \simeq \frac{\rho_1}{\rho_2}\left[\frac{1}{1 + |U_1^*U_2|/n}\right]\cdot\left[\frac{1}{1 - |U_1^*U_2|/n}\right] . \quad (11)
$$

When $|U_1^*U_2|/n$ approaches 1 it is seen from (9) and (11) that the eigenvalue disparity (i.e., the ratio $\lambda_{max}/\lambda_{min}$) increases without bound, regardless of the disparity in jammer power levels (i.e., the ratio ρ_1/ρ_2). The eigenvalue disparity in (11) is approximately 0.25 ρ_1/ρ_2 times the eigenvalue disparity in (9). It may be observed from (10) that the high-power jammer determines the largest eigenvalue. This implies [according to (3)] that the high-power jammer is attenuated quickly. From (10) it is also seen that the smaller eigenvalue is determined by the low-power jammer, by the angular separation between the jammers, and by the array configuration. Thus for $|U_1^*U_2|/n$ approaching 1, we see that this eigenvalue becomes quite small. This explains why the low-power jammer was attenuated very slowly in Fig. 2.

When $|U_1^*U_2|/n$ approaches 0 it is seen from (8) that both the eigenvalues are the same and hence the ratio $\lambda_{max}/\lambda_{min}$ approaches 1. The same ratio in class (ii) becomes only ρ_1/ρ_2.

To summarize the above, it may be stated that the eigenvalue disparity varies between ρ_1/ρ_2 and ∞ as $|U_1^*U_2|/n$ varies between 0 and 1. $|U_1^*U_2|/n$ in turn depends upon the angular positions (ψ_1,ψ_2) of the two jammers and on the number of antenna elements and their geometrical arrangement. For a given range of values of ψ_1 and ψ_2, the number of elements and their arrangement may be chosen such that $|U_1^*U_2|/n$ may be kept small, which in turn will keep the eigenvalue disparity near the jammer power disparity.

Examples of various array configurations are examined in the next section in order to study their effect on the eigenvalue disparity.

IV. ESTIMATING RELATIVE CONVERGENCE RATES IN VARIOUS ARRAY CONFIGURATIONS

Several antenna array configurations were tried in order to study the eigenvalue disparity. Some of these configurations have been shown in Figs. 1, 5a and 6a. For the configurations in Figs. 5a and 6a the phase shifters and the adaptive linear combiner have not been shown, but are assumed to be present as before.

Figures 4, 5b, and 6b are plots of normalized eigenvalue disparity NED defined as $[\lambda_{max}/\lambda_{min}]/[\rho_1/\rho_2]$ for the corresponding configurations. In each case the position of jammer 1, i.e., ψ_1, is fixed arbitrarily at 40^0 while that of jammer 2, i.e., ψ_2, is varied between -180^0 and 180^0. Normalized eigenvalue disparity is plotted as a function of ψ_2.

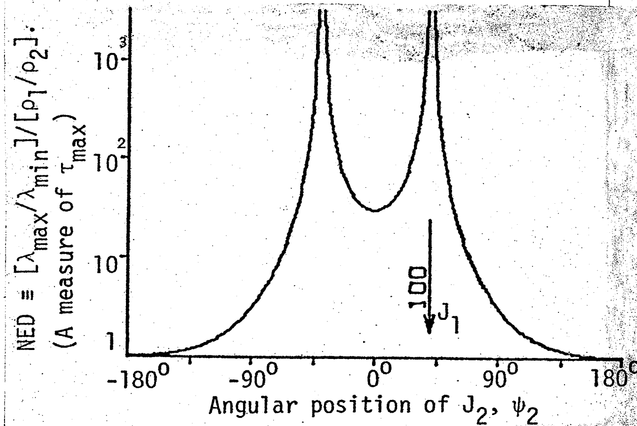

Fig. 4. Eigenvalue disparity for ANS of Fig. 1.

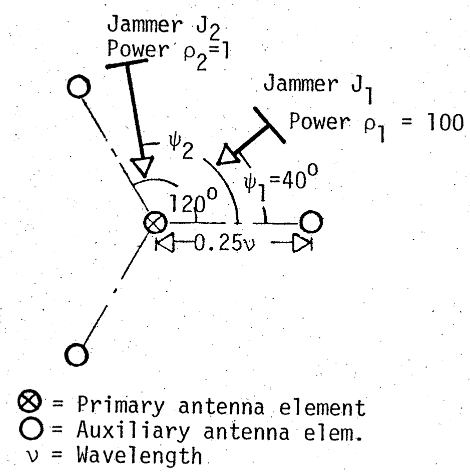

Fig. 5a. An array with 3 auxiliaries arranged in a triangle.

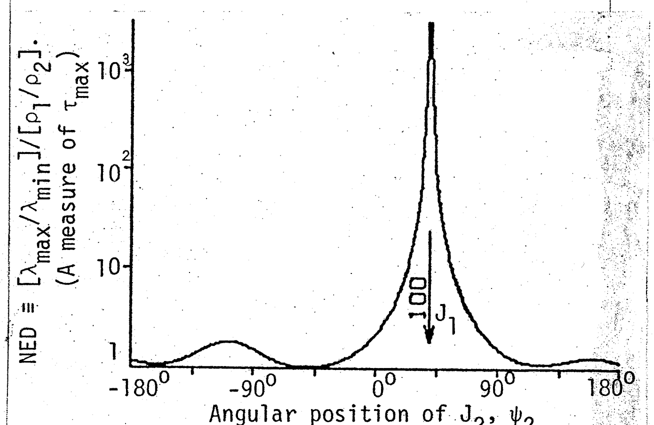

Fig. 5b. Eigenvalue disparity for the triangular configuration of Fig. 5a.

Comparing Figs. 4 and 5b it is evident that, in the region where $|\psi_1 - \psi_2|$ is small, the normalized eigenvalue disparity (NED) is substantially less for the triangular configuration (Fig. 5b) than the NED for the linear configuration with two auxiliary elements (Fig. 4). As a specific example, at $\psi_2 = 55^o$ the NED for the triangular configuration (Fig. 5b) is 12.5, while the NED for the linear configuration (Fig. 4) is 45.0. That is, the NED in the triangular configuration is 1/3.6 times the NED in the linear configuration. Using the lower bound on τ_{max} [i.e., (5)] it is estimated that the adaptive nulling process in the triangular configuration is about 3.6 times faster than that in the linear configuration.

The NED plot for a linear configuration with three auxiliary elements† is similar to the plot shown in Fig. 4, except that with the three auxiliary elements, the value of NED for each ψ_2 is smaller than the corresponding value in Fig. 4. At $\psi_2 = 55^o$, NED for the three auxiliary case is 17.1, which is 2.6 times smaller than the NED in the linear configuration with two auxiliaries. This indicates that the nulling process in the array with three auxiliaries will be correspondingly faster than that in the array with two auxiliaries.

Hexagonal configuration,† a natural extension of the triangular, was tried. In the region $-50^o \leqslant \psi_2 \leqslant 110^o$, the NED plot (not shown here) appears identical to that in Fig. 5b. In the other regions the NED is somewhat better (i.e., smaller) than that in Fig. 5b. Thus generally the hexagonal configuration may be expected to behave similarly to the triangular. At $\psi_2 = 55^o$ the NED is the same as in the triangular case and hence the convergence rate in both cases is expected to be the same.

Next consider the configuration shown in the Fig. 6a, which consists of two concentric triangles. The inner triangle is the same as that of Fig. 5a. The outer triangle has its vertices at a radius of 7.75 wavelengths (which is 30 times the radius of the inner one). The resulting NED plot is shown in Fig. 6b. Except for a very small region around 40^o (the position of Jammer 1) the value of NED rarely exceeds 10. For the example of $\psi_2 = 55^o$, the value of NED is 1.13. This values is approximately 11 times smaller than the corresponding NED for the single small triangle case (Fig. 5b). This

---

†These configurations and the corresponding NED plots are not shown due to space limitation.

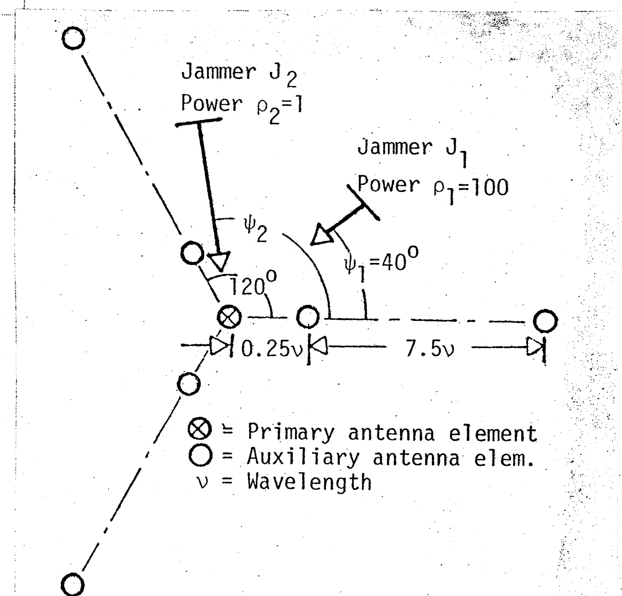

Fig. 6a. An array with 6 auxiliaries arranged in two concentric triangles.

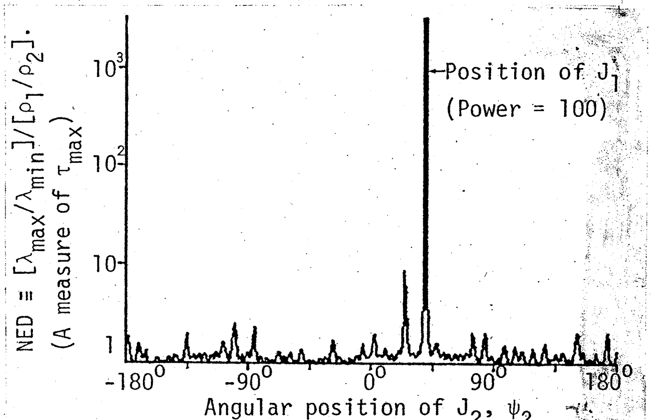

Fig. 6b. Eigenvalue disparity for the array with two concentric triangles (Fig. 6a).

indicates a correspondingly faster convergence rate in the two triangle case.

Comparing the two-triangle case (Fig. 6b) with the two-auxiliary-element linear configuration (Fig. 4) the NED in the two-triangle case is 40 times smaller than the corresponding NED in the linear case. Thus it appears that the nulling process in the two triangle case will be 40 times faster than that in the linear case.

The reasoning which led to the selection of the two-triangle case for study was as follows: It may be seen that elements spaced at a long distance from the primary element experience a large time difference in the signal. Hence *intuitively a large separation between elements (a large aperature) may tend to magnify the* *apparent angular separation between closely spaced jammers. This magnification tends to reduce the disparity between eigenvalues of the adaptive null steerer.* This explanation may be supported by examining relation (6) and (7) in detail (space limitation prohibits such an examination in this paper).

It should be recalled that the discussion relating the eigenvalue disparity for various configurations basically compares the lower bounds on τ_{max}. That such a comparison does give a good indication of the relative speed of convergence is confirmed by the results obtained from the simulations given in the following section.

V. SIMULATION RESULTS

Simulations for the cases discussed in Section IV were run in a manner similar to that discussed in Section II. The same simulation program was applied to all the arrays.

The results of the simulations have been summarized in Table I. For comparison, the estimated rate of convergence based on NED (as in Section IV) is also given in the table. The table includes data relating the cases not covered in the figures. Detailed discussion on the results of simulation follows.

The adaptation constant μ was set at 1×10^{-3} for the case in Fig. 1. The time sequence of beam patterns resulting therefrom is shown in Figs. 2a, b, c and d. The value of $\mu = 1 \times 10^{-3}$ was arrived at after a few experimental runs. A smaller value of μ resulted in a slower convergence rate than shown in Fig. 2, with no improvement in the pattern. A larger value of μ resulted in poor beam patterns. For other array configurations listed in the table, μ was set inversely proportional to the number of auxiliary elements in each case. If μ was set smaller than shown in the table, the adaptive nulling process would be slower than that obtained with the given μ, without any improvement in the beam pattern. If μ was set larger, the beam pattern would deteriorate in comparison with that obtained with the given μ.

In all cases the high-power jammer was nulled quickly while the other was nulled slowly. The definition of time of convergence is the same as that given in Section II -- i.e., the number of adapts required to reduce output power to below 1×10^{-6}. The beam pattern achieved at or below this power level is essentially that predicted by analysis. Analytical predictions of the beam pattern may be found in Mesiwala[8] and will also be a subject of a future report.

For the triangular array configuration, the observed convergence rate is six times as fast as the rate for the linear configuration of Fig. 1. It may be noted that the observed convergence rate is substantially faster than

Table I

CONVERGENCE RATE CHARACTERISTICS OF VARIOUS ARRAY CONFIGURATIONS

Array Configuration			Estimates From Lower Bound on τ_{max}		Simulation Data and Results		
Figure No.	Geometry of Auxiliary Elements	No. of Auxiliary Elements	NED $\equiv [\lambda_{max}/\lambda_{min}]/[\rho_1/\rho_2]$ at $\psi_1=40^o$, $\psi_2 = 55^o$	Relative Converg. Rates†	μ Used	No. of Adapts for Converg.	Relative Converg. Rates‡
Fig. 1	Line	2	44.97	--	$1\text{x}10^{-3}$	141,000	--
--	Line	3	17.11	2.6	$0.67\text{x}10^{-3}$	50,000	2.8
Fig. 5a	Triangle	3	12.50	3.6	$0.67\text{x}10^{-3}$	23,500	6.0
--	Hexagon	6	12.50	3.6	$0.33\text{x}10^{-3}$	23,500	6.0
Fig. 6a	Two concentric triangle	6	1.13	39.8	$0.33\text{x}10^{-3}$	3,900	36.2

† Estimated relative convergence rate $\triangleq \dfrac{\text{NED for linear array with 2 auxiliary elements}}{\text{NED for the configuration under consideration}}$

‡ Observed relative convergence rate $\triangleq \dfrac{\text{No. of adapts for linear array with 2 aux. elem.}}{\text{No. of adapts for the config. under consideration}}$

that estimated in Section IV by comparison of the lower bounds on τ_{max}. The converged beam pattern is shown in Fig. 7.

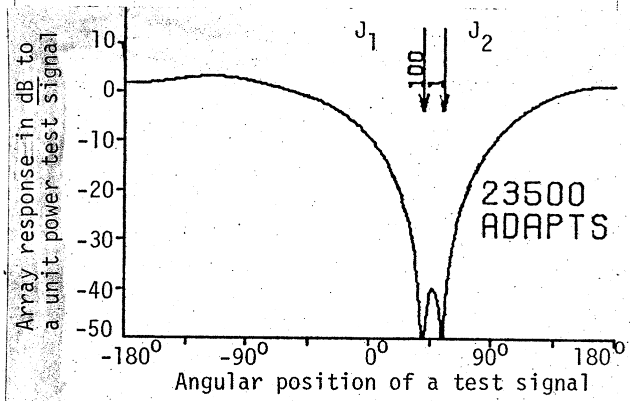

Fig. 7. Converged beam pattern for triangular configuration of Fig. 5a.

From Table 1 it is seen that the linear configuration with three auxiliaries converged 2.8 times as fast as the case in Fig. 1. This is slightly faster than that estimated on the basis of lower bound on τ_{max}. The converged beam pattern (not shown) was similar to that in Fig. 2d. The pattern showed similar notches in the jammer positions and it was slightly better in other regions.

The results of simulation of the hexagonal configuration were essentially the same as that for the triangular. The convergence rate was the same as for the triangular case. The beam pattern was strikingly similar to that shown in Fig. 7.

The observed convergence rate in the two concentric triangle configuration was about 36 times as fast as that in the case in Fig. 1. This rate is slightly lower than estimated on the basis of lower bound on τ_{max}. The converged beam pattern is shown in Fig. 8.

Thus far the discussion has centered on the rate of convergence, but not on the characteristics of converged beam patterns. Starting with a linear configuration with two auxiliaries, it is seen that the pattern (Fig. 2d) lacks omnidirectionality. Merely adding an extra element does not improve the pattern substantially as was discussed for the case of linear array with three auxiliaries; but rearranging the three auxiliary elements in a triangle yields a more omnidirectional beam pattern as seen by comparing Fig. 7 with Fig. 2d. Simply extending the triangular configuration into a hexagonal one by adding three more elements does not change the beam pattern substantially

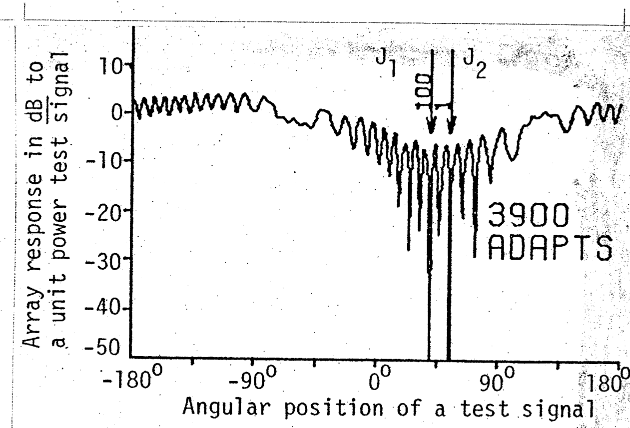

Fig. 8. Converged beam pattern for the array with two concentric triangles (Fig. 6a).

(as stated before); but forming two concentric triangles with six elements does change the pattern substantially -- see Figs. 7 and 8. In Fig. 8 the notches in the locations of jammers are sharp and the pattern between the two notches is more omnidirectional than in Fig. 7. It is conjectured that the presence of extra notches in Fig. 8 could be minimized by adding a few extra elements and/or by rearranging the geometry of the array.

VI. CONCLUSION AND DIRECTION FOR FURTHER STUDY

It has been demonstrated that the addition and judicious placement of a few extra auxiliary elements speeds up the adaptive nulling process and improves the beam pattern of a minimal adaptive antenna array system subjected to two closely spaced jammers of disparate power levels.

Further work is needed to investigate different adaptive processors to improve convergence rate even further. In such a case the additional elements may then be used to tailor the beam pattern according to particular requirements. Work is proceeding in this direction and will be reported in the future.

ACKNOWLEDGMENT

The authors wish to thank Mrs. Mabel Rockwell for her assistance in editing this paper and Mieko Parker for typing and assembling this manuscript.

APPENDIX

The purpose of this appendix is to obtain explicit expressions for the eigenvalues of the adaptive antenna array in Fig. 3.

Let the two jammers arriving at angles ψ_1 and ψ_2 be sinusoids. Let the weights attached directly to the antenna elements be labeled 1 through n, and those attached after the -90^0 phase shift be correspondingly labeled n + 1 through 2n. See Fig. 3.

The signal at the input to k^{th} weight is given by

$$\left.\begin{aligned} x_k &= \sqrt{2\rho_1}\cos(\omega_1 t+\theta_1-\phi_{k1}) \\ &\quad + \sqrt{2\rho_2}\cos(\omega_2 t+\theta_2-\phi_{k2}) \end{aligned}\right\}$$

where, for i = 1, 2 we have

$\rho_i \triangleq$ Jammer power i at each ant. ele.

$\omega_i \triangleq$ Radian frequency of jammer i.

$\theta_i \triangleq$ Uniformly distributed $[0,2\pi]$ random phase of the jammer i at the primary element. (θ_1 is statistically independent of θ_2.)

$$\phi_{ki} = \begin{cases} 2\pi\ell_k \cos(\psi_i-\alpha_k) & \text{for } k = 1,\ldots,n \\ 2\pi\ell_{k-n}\cos(\psi_i-\alpha_{k-n}) - \frac{\pi}{2} & \text{for } k = n+1,\ldots,2n \end{cases} \qquad \text{(A1)}$$

It can be seen that

$$E(x_j x_k) = \rho_1\cos(\phi_{j1}-\phi_{k1}) + \rho_2\cos(\phi_{j2}-\phi_{k2})$$
$$\text{for } j,\ k=1,\ \ldots,\ 2n \quad . \qquad \text{(A2)}$$

The correlation matrix R is defined by

$$R \triangleq [E(x_j x_k)] \quad . \qquad \text{(A3)}$$

Substituting from (A1) and (A2):

$$R = \left[\begin{array}{c|c} C_1+C_2 & +(D_1+D_2) \\ \hline -(D_1+D_2) & C_1+C_2 \end{array}\right] \qquad \text{(A4)}$$

where C_1, C_2, D_1 and D_2 are nxn matrices given by

$$[C_i]_{jk} = \rho_i\cos(\phi_{ji}-\phi_{ki})$$
$$[D_i]_{jk} = \rho_i\sin(\phi_{ji}-\phi_{ki})$$
$$i = 1,\ 2$$
$$j,\ k = 1,\ \ldots,\ n$$

The eigenvalues of R are related to the eigenvalues of a complex matrix B given by

$$B \triangleq C_1 + C_2 + i[-(D_1+D_2)] \qquad \text{(A5)}$$

in the following manner[8]: n eigenvalues (say $\lambda_1, \lambda_2, \ldots, \lambda_n$) of R are the same as those of B. The remaining n eigenvalues are related as follows:

$$\lambda_k = \lambda_{k-n} \quad \text{for} \quad k = n+1,\ \ldots,\ 2n \quad . \qquad \text{(A6)}$$

Writing B in terms of vector outer products of complex exponential vectors:

$$B = \rho_1 U_1 U_1^* + \rho_2 U_2 U_2^*$$

where

$$U_j = \left[e^{-i\phi_{1j}},\ e^{-i\phi_{2j}},\ \ldots,\ e^{-i\phi_{nj}}\right]^T \qquad j = 1,2 \quad . \qquad \text{(A7)}$$

From (A7) it is evident that B is hermitian and of rank $\leqslant 2$ for $n \geqslant 2$. Thus B has at most two positive eigenvalues. All other eigenvalues are zero. The two eigenvectors corresponding to the nonzero eigenvalues are in the space spanned by U_1 and U_2. Thus an eigenvector is given by

$$\Gamma = \gamma_1 U_1 + \gamma_2 U_2 \qquad \text{(A8)}$$

where γ_1 and γ_2 are complex scalars to be determined from the following derivation. Now,

$$B\Gamma = \gamma_1 U_1\left[\rho_1\left(n + \frac{\gamma_2}{\gamma_1}U_1^* U_2\right)\right] + \gamma_2 U_2\left[\rho_2\left(n + \frac{\gamma_1}{\gamma_2}U_2^* U_1\right)\right] . \qquad \text{(A9)}$$

For Γ to be an eigenvector it is necessary that

$$\lambda \triangleq \rho_1\left(n + \frac{\gamma_2}{\gamma_1}U_1^* U_2\right) = \rho_2\left(n + \frac{\gamma_1}{\gamma_2}U_2^* U_1\right) . \qquad \text{(A10)}$$

Solving (A10):

$$\frac{\gamma_2}{\gamma_1} = \frac{\frac{n}{2}(\rho_2-\rho_1)\pm\left[\frac{n^2}{4}(\rho_2-\rho_1)^2+\rho_2\rho_1|U_1^*U_2|^2\right]^{\frac{1}{2}}}{\rho_1 U_1^* U_2} \qquad \text{(A11)}$$

Substituting (A11) in (A10) and using (A6),

$$\left.\begin{aligned}
\lambda_1 &= \frac{n}{2}(\rho_1+\rho_2)+\left[\frac{n^2}{4}(\rho_1-\rho_2)^2+\rho_1\rho_2|U_1^*U_2|^2\right]^{\frac{1}{2}} \\
\lambda_2 &= \frac{n}{4}(\rho_1+\rho_2)-\left[\frac{n^2}{4}(\rho_1-\rho_2)^2+\rho_1\rho_2|U_1^*U_2|^2\right]^{\frac{1}{2}} \\
\lambda_{n+1} &= \lambda_1;\ \lambda_{n+2} = \lambda_2 \\
\lambda_m &= 0 \quad \text{for} \quad m \notin \{1, 2, n+1, n+2\} \quad .
\end{aligned}\right\} \qquad \text{(A12)}$$

Thus the eigenvalues for the configuration of Fig. 3 have been obtained.

REFERENCES

1. B. Widrow, P. E. Mantey, L. J. Griffiths and B. B. Goode, "Adaptive antenna systems," Proc. IEEE, vol. 55, pp. 2143-2159, Dec. 1967.

2. C. L. Zahm, "Application of adaptive arrays to suppress strong jammers in the presence of weak signals," IEEE Trans. on Aerospace and Electronic Systems, vol. AES-9, pp. 260-271, March 1973.

3. L. J. Griffiths, "A simple adaptive algorithm for real-time processing in antenna arrays," Proc. IEEE, vol. 57, pp. 1696-1704, Oct. 1969.

4. O. L. Frost, "An algorithm for linearly constrained adaptive array processing," Proc. IEEE, vol. 60, pp. 926-935, Aug. 1972.

5. W. D. White, "Cascade preprocessors for adaptive antennas," IEEE Tran. Antenna and Propagation, vol. AP-24, pp. 670-684, Sept. 1976.

6. I. S. Reed, J. D. Mallet and L. E. Brennan, "Rapid convergence rate in adaptive arrays," IEEE Trans. Aerospace and Electronic Systems, vol. AES-10, pp. 853-863, Nov. 1974.

7. B. Widrow, J. M. McCool, M. G. Larimore and R. Johnson, Jr., "Stationary and nonstationary learning characteristics of the LMS adaptive filter," Proc. IEEE, vol. 64, pp. 1151-1162, Aug. 1976.

8. H. M. Mesiwala, Ph.D. dissertation, Department of Electrical Engineering, Stanford University, Stanford, CA, June 1979.